Six-quasiparticle isomer in ^{140}Nd

C. M. Petrache,[1] R. A. Bark,[2] S. T. H. Murray,[2] M. Fantuzi,[1] E. A. Lawrie,[2] S. Lang,[2,3] J. J. Lawrie,[2] S. M. Maliage,[2,3]
D. Mengoni,[1] S. M. Mullins,[2] S. S. Ntshangase,[2,4] D. Petrache,[1] T. M. Ramashidzha,[2,3] and I. Ragnarsson[5]

[1]*Dipartimento di Fisica, Università di Camerino and INFN, Sezione di Perugia, I-62032, Camerino, Italy*
[2]*iThemba LABS, PO Box 722, Somerset West 7129, South Africa*
[3]*University of the Western Cape Bellville 7535, South Africa*
[4]*Dept. of Physics, University of Zululand, Private Bag X1001, KwaDlangezwa, 3886, South Africa*
[5]*Department of Mathematical Physics, Lund Institute of Technology, S-22362 Lund, Sweden*

A search for isomeric states was performed in the nucleus $^{140}_{60}$Nd$_{80}$ using in-beam γ-ray spectroscopy and the
^{126}Te(^{18}O,$4n$) reaction. Prompt and delayed γ-ray coincidences were measured with the AFRODITE spectrometer
using the pulsed beam delivered by the Separated Sector Cyclotron of iThemba LABS. One new isomer was
identified, with spin-parity $I^\pi = 20^+$ and lifetime $T_{1/2} \geqslant 400$ ns, at an excitation energy $E_x = 7430$ keV. The
lifetime of the 10^+ isomer at $E_x = 3619$ keV was determined to be 32.9(1.8) ns, confirming the previously
reported value. The configuration of the $I^\pi = 20^+$ isomer is assigned based on configuration-dependent cranked
Nilsson-Strutinsky (CNS) calculations as a state $\pi(d_{5/2}g_{7/2})^{-4}_{10^+} \otimes \nu(h^{-2}_{11/2})_{10^+}$, with the spin vectors of the six
holes in the $^{146}_{64}$Gd$_{82}$ core fully aligned.

I. INTRODUCTION

The nuclei around the $N = 82$ shell closure are a fertile field
of spectroscopic investigations both at low and high spins: at
low spins the presence of isomers based on simple particle-
hole configurations helps to establish the active quasiparticle
configurations in a specific nucleus and test the suitability
of various nuclear potentials [1], whereas at high spins the
combined contribution of neutron holes and proton particles
drive the nuclear shape toward a stable triaxial shape with $\gamma \approx$
$+30°$ [2,3]. At very high spins superdeformation is observed
[4]. To give a realistic interpretation of the observed bands
at high spins one needs to know the linking transitions of
the bands to low-lying structures and their characteristics and,
of course, the spins and parities of the low-lying states. In
all high-spin experiments, the detailed study of the low-spin
structure of the nuclei is a prerequisite for the understanding
of the high-spin structures, whose excitation energy, spin, and
parity depend on the low-spin states.

The task of determining the characteristics of the low-lying
states in the nearly spherical nuclei close to the shell closures
is more difficult than in the well-deformed nuclei due to the
presence of isomeric states, which often stops and fragments
the decay flux. The analysis of the data coming from large
γ arrays such as GASP, Euroball, and Gammasphere is
made difficult by the presence of low-energy γ rays and
isomeric states that often are not measured in the performed
experiments. Such a situation is encountered in the weakly
deformed Nd nuclei with neutron numbers close to the $N =$
82 shell closure, with irregular sequences of transitions and
possible yrast traps. In fact, isomeric states were observed
in ^{138}Nd ($I^\pi = 10^+$, $T_{1/2} = 410$ ns) [5] and ^{140}Nd ($I^\pi =$
10^+, $T_{1/2} = 32$ ns and $I^\pi = 7^-$, $T_{1/2} = 600$ μs) [6]. In the
odd-even Nd nuclei the information about the isomeric states
is much more limited: a $I^\pi = 19/2^+$, $T_{1/2} = 4$ ns isomer is
known in ^{137}Nd [7], in ^{139}Nd there exist only indications about

the existence of an isomer with $T_{1/2} \geqslant 141$ ns [8], whereas in
^{141}Nd the information on isomeric states is lacking completely.

The study of the isomeric decay in these nuclei is very
important for the understanding of the quasiparticle excitations
into the orbitals closest to the Fermi surface, whereas the
search for high-spin isomers in needed to test the theoretical
model predictions of multiquasiparticle configurations, as, for
example, the recent CNS predictions of the favored high-spin
configurations in ^{140}Nd [3,9].

In this work we report results on isomeric states in ^{140}Nd
obtained from prompt and delayed $\gamma\gamma$ coincidences measured
in a pulsed-beam experiment. Previously, the level scheme of
^{140}Nd was studied both at low [3,6] and at high spins [3,9].

In Secs. II and III the experimental details and results will
be presented. In Sec. IV the structure of the new identified
isomer in ^{140}Nd will be discussed including a survey of our
present understanding of the ^{140}Nd level scheme in its full
spin range from the ground state to the superdeformed bands
beyond $I = 60$. Finally, the present results are summarized in
Sec. V.

II. EXPERIMENTAL DETAILS

High-spin states in ^{140}Nd have been populated in the
reaction ^{126}Te(^{18}O,$4n$) with a 70 MeV ^{18}O beam delivered
by the Separated Sector Cyclotron accelerator at iThemba
LABS, South Africa. The target was ^{126}Te with a thickness of
400 μg/cm^2 on a 5-mg/cm^2-thick Au backing. γ-ray coinci-
dences were measured with the AFRODITE spectrometer [10],
consisting of eight Clover Ge detectors with BGO Compton-
suppression shields and six segmented LEPS detectors. Events
were written on tape with the requirement that at least two
Compton-suppressed Clover detectors were in coincidence.
The reaction yield was dominated by the $4n$ channel, leading
to the nucleus of interest ^{140}Nd with a cross section of

around 1 mb. The thick Au target backing was used to stop the recoiling nuclei in the center of the array to measure the isomeric decay. The cyclotron pulsing period was about 80 ns; by selecting every fifth pulse we obtained $\approx$400 ns between pulses, a time interval sufficient to study isomers with lifetimes in the range of tens of nanoseconds. We have measured delayed coincidences (measured relative to the cyclotron RF), as well as prompt and prompt-delayed coincidences, to study cascades built either above or below possible isomeric states. The use of large-volume Clover detectors with good efficiency and resolution for high-energy γ rays and of LEPS detectors with good efficiency for low-energy transitions allowed us to efficiently study coincidences between high- and low-energy γ rays, which are very likely to occur in the weakly deformed Nd nuclei near $N = 82$, expected to have an irregular level structure at low and medium spins. Moreover, the use of the LEPS detectors enables the assignment of the possible new observed cascades below the isomer to a specific element through the conversion x rays detected in coincidence with other γ rays in the cascade.

The γ-ray coincidences were sorted into two-dimensional coincidence arrays and the analysis was carried out using the RADWARE software package [11]. A total of 500×10^6 events with a γ-ray coincidence fold $f \geqslant 2$ was obtained from the data, which were sorted including the add-back for the composite detectors.

III. RESULTS AND LEVEL SCHEME

In this section the results obtained in our experiment for ^{140}Nd are presented. The level scheme of ^{140}Nd has been studied in detail and extended to very high spins recently using prompt coincidence techniques [3]. The study of the isomeric states was done much earlier, resulting in the identification of three isomers with lifetimes between 0.25 ns and 0.6 ms, as follows: a $I^\pi = 7^-$ state at $E_x = 2221$ keV with $T_{1/2} = 0.6$ ms [12], a $I^\pi = 10^+$ state at $E_x = 3619$ keV with $T_{1/2} = 32(1)$ ns [6,13] and possibly an $I = 12$ isomer at $E_x = 4512$ keV with $T_{1/2} = 0.25$ ns [14].

A partial level scheme resulting from the present experiment dedicated to the study of isomeric transitions is shown in Fig. 1. Note that the 281 keV $(19^- \rightarrow 18^-)$, 818 keV $(8^+ \rightarrow 6^+)$, 963 keV $(8^+ \rightarrow 7^-)$, and 971 keV $(10^+ \rightarrow 8^+)$ transitions are not seen in the delayed spectra and therefore are drawn with dashed lines in Fig. 1; these transitions are instead present in the level scheme reported in Fig. 1 of Ref. [3], obtained from the analysis of only prompt coincidences. Details on the observed transitions in ^{140}Nd, including their energy and delayed intensity from the present experiment, as well as the DCO ratios from the prompt coincidence data reported in Ref. [3] and the spin-parity assignments, are given in Table I. Our analysis revealed one new isomer at $E_x = 7430$ keV, most probably with $I^\pi = 20^+$ and $T_{1/2} \geqslant 400$ ns, as it will be shown in the discussion of Sec. IV. Examples of delayed γ-ray coincidence spectra and time spectra for the new isomers are displayed in Figs. 2–5.

In Fig. 2 we show the delayed spectra gated on the newly observed γ rays of 228 and 341 keV, deexciting the isomeric

TABLE I. γ-ray energies and delayed intensities for transitions in ^{140}Nd from the present experiment, together with the DCO ratios from the prompt coincidence data reported in Ref. [3].

E_γ(keV)[a]	Transition intensities[b]	DCO ratios[c]	Assignment $I_i^\pi \rightarrow I_f^\pi$
90.5	11		$6^+ \rightarrow 5^-$
119.7	11		$14^- \rightarrow 13^-$
143.9	9		$6^+ \rightarrow 7^-$
149.7	1		$18^- \rightarrow 17^-$
165.9	13		$10^+ \rightarrow 9^-$
173.5	11	0.56(2)	$13^- \rightarrow 12^-$
181.6	11		$15^- \rightarrow 14^-$
183.5	2	0.53(2)	$12^- \rightarrow 11^{(-)}$
188.3	31		$13^- \rightarrow 12^-$
190.9	31	0.68(2)	$12^- \rightarrow 11^-$
203.0	1		$17^- \rightarrow 16^-$
211.8	11	0.59(3)	$15^- \rightarrow 14^-$
212.9	11		$13^- \rightarrow 12^-$
216.0	49		$9^- \rightarrow 8^-$
216.3	1		$10^- \rightarrow 9^-$
220.2	3	0.56(3)	$12^- \rightarrow 11^-$
222.4	1		$12^- \rightarrow 11^{(-)}$
227.5	10		$20^+ \rightarrow 18^-$
240.6	4	0.59(1)	$18^- \rightarrow 17^-$
258.4	22	0.57(8)	$16^- \rightarrow 15^-$
287.7	2		$16^- \rightarrow 15^-$
292.0	11		$11^- \rightarrow 10^-$
341.0	2		$18^+ \rightarrow 17^-$
420.0	90		$7^- \rightarrow 4^+$
431.0	10		$18^+ \rightarrow 17^-$
436.0	1		$12^- \rightarrow 13^-$
437.3	13		$17^- \rightarrow 15^-$
473.7	1		$5^- \rightarrow 4^+$
482.8	5	1.03(5)	$12^- \rightarrow 10^-$
505.0	16	0.55(8)	$17^- \rightarrow 16^-$
544.3	3	0.46(2)	$16^- \rightarrow 15^-$
554.3	2		$10^- \rightarrow 10^+$
564.2	2		$6^+ \rightarrow 4^+$
575.9	11		$10^- \rightarrow 9^-$
608.2	4	0.62(7)	$13^- \rightarrow 13^-$
695.0	5		$7^- \rightarrow 6^+$
700.7	1		$11^- \rightarrow 10^+$
702.2	1	0.33(4)	$11^- \rightarrow 10^-$
718.6	4		$9^- \rightarrow 8^-$
720.3	13		$10^- \rightarrow 9^-$
728.1	22	0.66(2)	$14^- \rightarrow 13^-$
772.6	100		$2^+ \rightarrow 0^+$
791.2	7		$10^- \rightarrow 8^-$
796.9	4	0.60(2)	$13^- \rightarrow 12^-$
798.0	3		$18^- \rightarrow 17^-$
807.0	1		$17^- \rightarrow 16^-$
840.0	22		$7^- \rightarrow 7^-$
867.8	31	1.12(3)	$11^- \rightarrow 9^-$
895.6	1		$9^- \rightarrow 7^-$
922.4	13	1.04(5)	$12^- \rightarrow 10^-$
962.7	5	1.04(12)	$12^- \rightarrow 10^-$
989.0	8		$18^+ \rightarrow 17^-$
1016.5	53	0.44(5)	$8^- \rightarrow 7^-$

TABLE I. (*Continued.*)

E_γ(keV)[a]	Transition intensities[b]	DCO ratios[c]	Assignment $I_i^\pi \to I_f^\pi$
1027.1	13		$20^+ \to 17^-$
1028.0	100		$4^+ \to 2^+$
1048.0	2	1.16(21)	$18^- \to 16^-$
1064.0	<1		$17^- \to 16^-$
1148.2	<1		$16^- \to 15^-$
1232.3	5	0.96(19)	$9^- \to 7^-$
1256.0	1		$11^- \to 10^+$
1267.0	13		$15^- \to 13^-$
1292.8	3	0.33(3)	$11^{(-)} \to 10^+$
1321.0	2	1.02(28)	$17^- \to 15^-$
1352.2	11	1.16(11)	$17^- \to 15^-$
1412.0	<1		$17^- \to 15^-$
1442.2	9	1.04(12)	$17^- \to 15^-$
1495.0	7		$18^+ \to 16^-$

[a]The intensities are normalized to the delayed intensity of the 772.6-keV ($2^+ \to 0^+$) transition. The error on the transition energies is 0.2 keV for transitions below 1000 keV and intensities larger that 5% of the ^{128}Nd channel, 0.5 keV for transitions above 1000 keV and intensities lower than 5%, and 1 keV for transitions above 1200 keV and/or weaker than 1%.

[b]Relative intensities corrected for efficiency. The transition intensities were obtained from a combination of total projection and gated spectra.

[c]The DCO ratios are obtained from the data of Ref. [3] and have been deduced from an asymmetric $\gamma\gamma$ coincidence matrix with a gate on an $E2$ trannsitions. The tentative spin - parity of the states are given in parenthesis.

state with $E_x = 7430$ keV and the state below it with $E_x = 7393$ keV, respectively. One can see that the 281 keV ($19^- \to 18^-$) γ ray observed previously in prompt coincidence with the lower-lying transitions of ^{140}Nd (see Fig. 1 in Ref. [3]) is missing in both spectra. In the spectrum of the 228 keV γ ray one can see all transitions below the 18^- state, from the highest-lying 150- and 240-keV transitions down to the ground state, whereas in the spectrum gated on the 341-keV transition the 150- and 240-keV peaks are not present, and one can see only the γ rays below the 17^- state populated by the 150-keV transition. These spectra, corroborated with the spectra gated on the new 431 keV γ-ray and on the other lower-lying transitions in the level scheme suggest the presence of isomeric states with $E_x = 7430$ keV and $E_x = 7393$ keV.

In Fig. 3 we show the delayed spectra gated on the previously known 258- and 505-keV transitions of the relatively intense cascade in the left-hand side of the level scheme. The 228-keV γ ray is seen in these gates through the connecting 1495-, 1064-, 1027-, 989-, and 798-keV γ rays from the newly identified states or from the previously known states of the right-hand side cascade.

In Fig. 4 we show the delayed spectra gated on the 240- and 281-keV γ rays. In the spectrum of the 240-keV γ ray one can see a strong 228-keV peak. All other peaks present in the spectrum belong to the already known level scheme of ^{140}Nd, indicating that the isomeric state is the state with $E_x = 7430$ keV, which can account for most of the measured
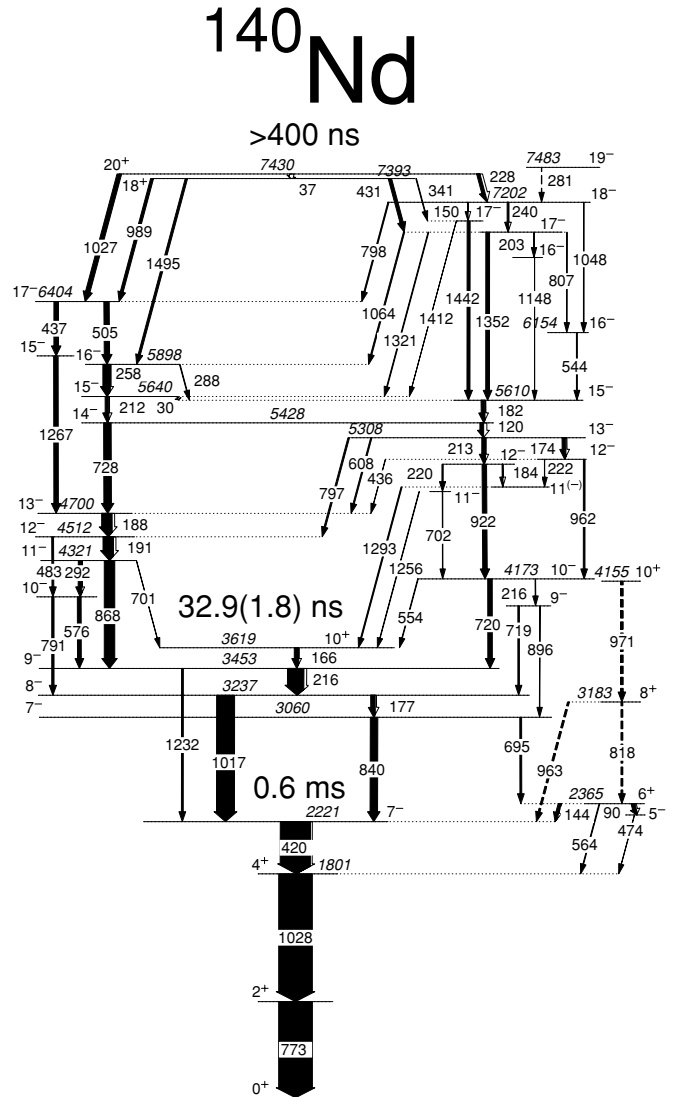

FIG. 1. Level scheme of ^{140}Nd below the new 20^+ isomer resulting from the analysis of the delayed coincidences. The arrow width is proportional to the observed intensity between the beam pulses. The dashed transitions were not seen in the present pulsed beam experiment, but in the spectra of the previous Euroball experiment reported in Ref. [3].

delayed coincidences. The spectrum gated on 281-keV instead has a very weak statistics and shows only statistical fluctuations resulting from the background subtraction around the strong peaks with energies of 436-, 511-, and 773-keV transitions. Therefore, the 281-keV γ ray is not in coincidence with the delayed 240-keV γ ray. This excludes the possibility that the isomeric state lies above the 19^- state.

In Fig. 5 we show the time spectra of the delayed γ rays measured relative to the radiofrequency signal from the cyclotron for several representative transitions: the spectrum of the 228-keV γ ray deexciting the $E_x = 7430$-keV state overlapped with that of the 420-keV γ ray deexciting the 7^- state with $T_{1/2} = 0.6$ ms, the spectrum of the 228-keV γ ray overlapped with that of the 341-keV γ ray deexciting the $E_x = 7393$-keV state below the isomeric state, and for
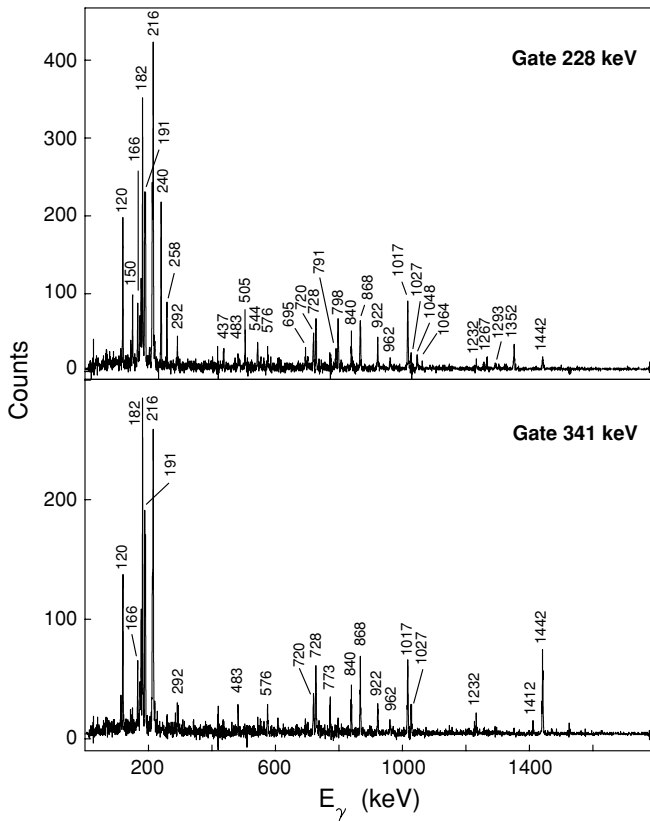
FIG. 2. Delayed coincidence spectra of the 228- and 341-keV γ rays deexciting the new isomeric state in ^{140}Nd with $I^\pi = 20^+$ at $E_x = 7430$ keV and of the state with $I^\pi = 18^+$ at $E_x = 7393$ keV.
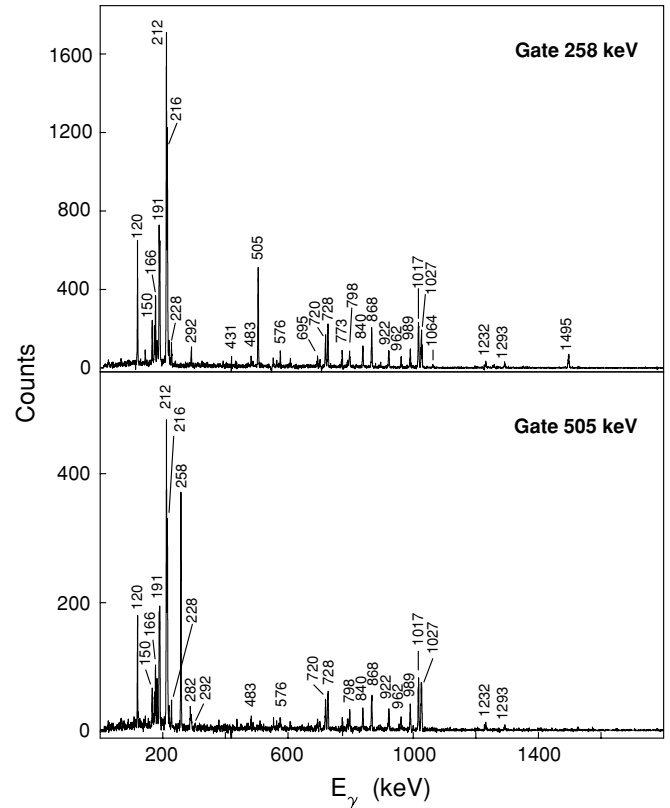

FIG. 3. Delayed coincidence spectra of the 258- and 505-keV γ rays deexciting the 16^- and 17^- states, respectively, of the left-hand-side cascade in ^{140}Nd.

comparison the spectrum of the 828-keV γ ray ($22^- \rightarrow 20^-$), which we published previously in Fig. 1 of Ref. [3]. One can see that the time spectrum of the 228-keV γ ray is nearly flat, such as the spectrum of the 420-keV γ ray, indicating a lifetime longer that the time interval of $\sim$400 ns between the beam pulses. The very similar time-difference spectra of the 228-keV transition deexciting the state with $E_x = 7430$ keV, and the corresponding spectra of the 341-, 431-, 989-, and 1495-keV transitions deexciting the newly identified state at $E_x = 7393$ keV suggest that the apparent lifetime of the newly identified states is due to the isomeric state with $E_x = 7430$ keV that feeds the $E_x = 7393$ keV state by an unobserved low-energy transition that is highly converted.

We therefore assign an isomeric character only to the state with $E_x = 7430$ keV.

The analysis of the delayed spectra from the isomeric state with $E_x = 7430$ keV that are much cleaner and with smaller background than the prompt spectra, lead to the identification of several new transitions: 895.6 keV ($9^- \rightarrow 7^-$), 216.3 keV ($10^- \rightarrow 9^-$), 436 keV ($12^- \rightarrow 13^-$), 222 keV ($12^- \rightarrow 11^-$), 30 keV ($15^- \rightarrow 15^-$), 288 keV($16^- \rightarrow 15^-$), 798 keV ($18^- \rightarrow 17^-$), 1064 keV ($17^- \rightarrow 16^-$), 1321 keV ($17^- \rightarrow 15^-$), 1412 keV ($17^- \rightarrow 15^-$), 203 keV ($17^- \rightarrow 16^-$), 1148 keV ($16^- \rightarrow 15^-$), 807 keV ($17^- \rightarrow 16^-$), and 1048 keV ($18^- \rightarrow 16^-$). This give confidence in the level scheme reported previously from a completely different experiment performed with the Euroball array [3].

We have also determined the half-life of the 10^+ isomer at $E_x = 3619$ keV by fitting an exponential decay to the sum of three time difference spectra constructed using the 1293-keV transition above the 3619-keV level as a "start" transition and the 166-, 1017-, and 840-keV transitions below the 3619-keV level as "stop" transitions, as shown in Fig. 6. The fitting interval was limited to lie within the electronic coincidence window of 190 ns. A half-life of 32.9(1.8) ns was obtained in good agreement with the earlier measurements [6,13].

We will now try to understand the observed deexcitation patterns of the newly observed states with $E_x = 7430$ and $E_x = 7393$ keV. The state with $E_x = 7393$ keV decays toward three states with spin 17^- and one state with spin 16^-, whereas the state with $E_x = 7430$ keV decays toward two yrast states with spins 17^- and 18^-.

The state with $E_x = 7430$ keV decays by means of the 228- and 1027-keV transitions and a possible low-energy 37-keV transition toward the state with $E_x = 7393$ keV. The single-particle Weisskopf estimates for the lifetime of the 228-keV γ transition is 19 μs for $M2$ character and 21 ns for $E2$ character. Only the 19-μs lifetime is in agreement with the time spectrum of the 228-keV transition shown in Fig. 5. The single-particle Weisskopf estimates for the lifetime of the 1027-keV γ transition is 0.84 μs for $E3$ character and 7.2 ms for $M3$ character, both supporting the $I^\pi = 20^+$ assignment. One should mention that the time spectrum of the 1027-keV transition could not be obtained, due to the contamination by
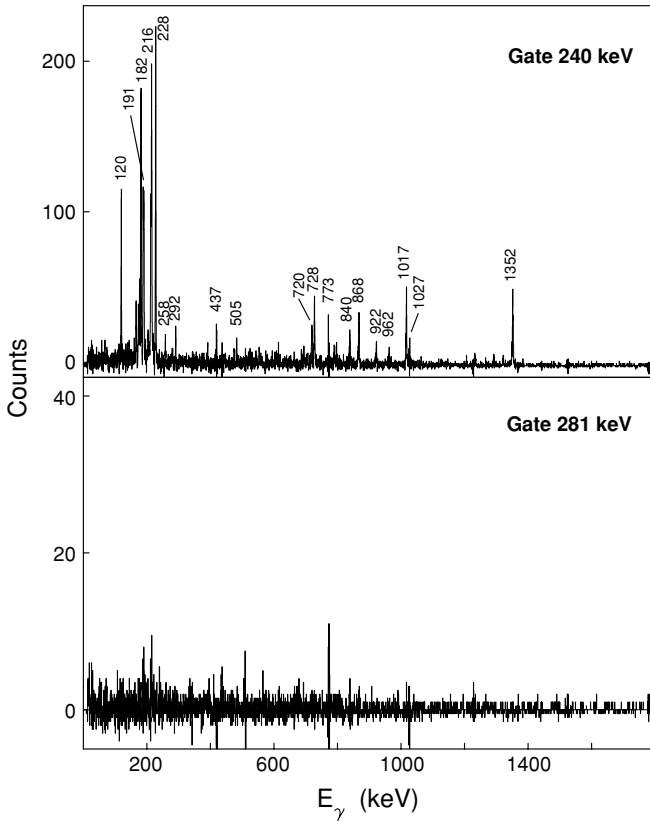
FIG. 4. Delayed coincidence spectra of the 240- and 281-keV γ rays deexciting 18^- and 19^- states, respectively, of the left-hand-side cascade in ^{140}Nd.

FIG. 5. Background subtracted spectra of the time of selected γ rays in ^{140}Nd measured relative to the radiofrequency signal from the cyclotron. The top panel shows the overlap of the time spectra of the 420- keV γ ray deexciting the 7^- isomeric state with $T_{1/2} = 0.6$ ms (thick line), and of the 228-keV γ ray deexciting the state with $E_x = 7430$ keV (thin line). The logarithmic scales for the 228- and 420-keV γ rays are on the left-hand side and right-hand side of the panel, respectively. The two lines indicate possible lower (400 ns) and upper (4000 ns) limits for the lifetime of the 20^+ state. The middle panel shows the time spectra of the 228-keV (thin line) and of the 989-keV (thick line) γ rays deexciting the newly observed isomer and the state with $E_x = 7393$ keV below the isomer, respectively. The logarithmic scales for the 228- and 989-keV γ rays are on the left-hand side and right-hand side of the panel, respectively. The bottom panel shows the time spectrum of the 828-keV γ ray ($20^- \rightarrow 18^-$) that we published previously in Fig. [1] of Ref. [3]. The bump at around 160 ns is due to the breakthrough of each second cyclotron pulse.

the 1028-keV ($2^+ \rightarrow 0^+$) transition below the $T_{1/2} = 0.6$ ms 7^- isomer. We assign therefore $I^\pi = 20^+$ to the state with $E_x = 7430$ keV.

Concerning the spin-parity of the state at $E_x = 7393$ keV, we have investigated the four possibilities leading to $I^\pi = 19^-, 18^-, 19^+, 18^+$. First of all, one should remember that for the 37-keV transition in ^{140}Nd, which has $Z = 60$, K-conversion is not energetically possible. L-conversion will lead to the emission of x rays with energies lower than 6 keV, which are below the electronic threshold of the LEPS detectors and therefore could not be observed experimentally.

We can immediately discard the $I^\pi = 19^-$ and $I^\pi = 18^-$ assignments based on the following simple argumentation. For the $I^\pi = 19^-$ case, the 37-keV transition should be $E1$, which has a total conversion coefficient $\alpha_T = 0.2$. The 37-keV transition would be only partially converted and be observed in the LEPS spectrum. After a careful inspection of the LEPS spectra in the low-energy region we have concluded that such a transition is not observed in the delayed spectra, and therefore the $I^\pi = 19^-$ assignment has been discarded. For the $I^\pi = 18^-$ case, the Weisskopf estimate of the partial lifetime for the 37-keV transition is 0.18 s, which is much longer than the $\sim$400 ns time interval between the beam pulses and prohibits the observation of the transitions deexciting the state at $E_x = 7393$ keV. The observation of the four transitions deexciting the state at $E_x = 7393$ keV in the $\sim$400 ns interval between beam
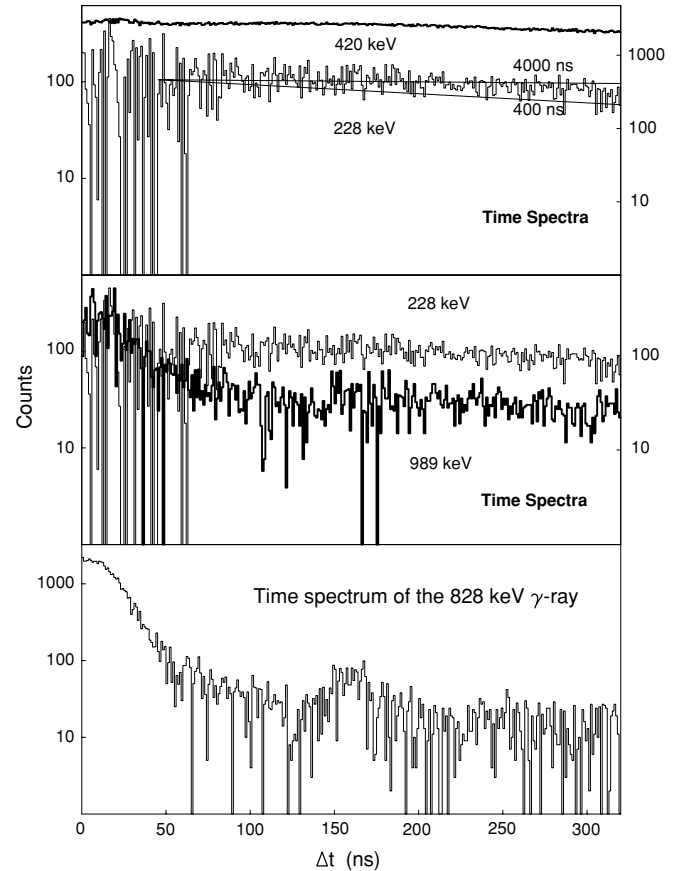
pulses indicates that also the $I^\pi = 18^-$ assignment should be discarded.

The $I^\pi = 19^+$ assignment, however, would lead to an $M1$ character for the 37-keV transition, nearly completely converted in the L shell ($\alpha_T = 2.8 \times 10^6$), with a Weisskopf estimate of the partial lifetime of 0.44 ns. This would lead to prompt feeding of the $E_x = 7393$-keV state. However, the time spectra of the transitions deexciting the state with $E_x = 7393$ keV, which look all similar, show lifetimes larger than the $\sim$400 ns interval between the beam pulses. This is also in disagreement with the predicted different lifetimes of the transitions deexciting the $I^\pi = 19^+$ state, as can be seen in
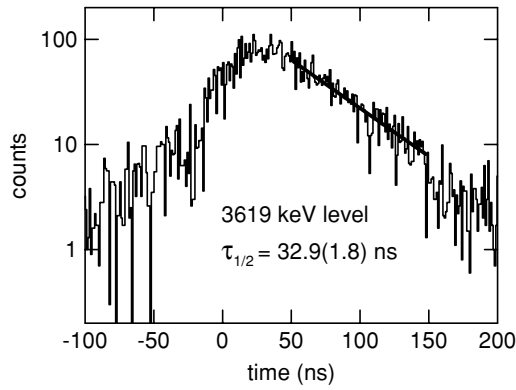
FIG. 6. The sum of three time-difference spectra constructed using the 1293-keV transition feeding the 3619-keV level as a "start" transition and the 166-, 1017-, and 840-keV transitions below the 3619-keV level as "stop" transitions. The solid line shows the exponential decay with a half-life of 32.9 ns, fitted to the data in the interval between 50 and 150 ns. The time $t = 0$ ns, corresponds to a prompt coincidence between γ rays of energy greater than $\simeq 500$ keV.

Table I, which lead to a Weisskopf estimate of the apparent lifetime of 39 ns. We can therefore also discard the $I^\pi = 19^+$ assignment.

The only plausible assignment is $I^\pi = 18^+$, which leads to an $E2$ character for the 37-keV transition, with a partial lifetime estimate of 185 μs. The four transitions deexciting the $I^\pi = 18^+$ state have estimated partial lifetimes smaller than 1 ns. Their time spectra showing a lifetime longer than $\sim$400 ns is therefore due to the delayed population from the $I^\pi = 20^+$ isomer. The $E1$, $M2$ and $E3$ transitions toward the negative parity states involve the jump of one neutron between the negative parity orbital $\nu h_{11/2}^{-1}$ and one of the positive parity orbitals $\nu d_{3/2}$, $\nu d_{5/2}$ and $\nu g_{7/2}$.

IV. DISCUSSION

A. The different coupling schemes observed in ^{140}Nd

To get a general overview of the different kind of states observed in ^{140}Nd, the low-lying expeimental states are plotted relative to a rotating liquid drop energy in the upper panel of Fig. 7. They are compared with calculated cranked Nilsson-Strutinsky (CNS) [15,16] configurations that are plotted in the lower panel. In the CNS formalism, pairing is neglected. Therefore, it becomes possible to specify configurations by the number of particles with signature $\alpha = 1/2$ and $\alpha = -1/2$, respectively, in the different shells (N_{rot} shells) of the rotating harmonic oscillator Hamiltonian. Furthermore, a distinction is made between orbitals dominated by high-j intruder subshells and other subshells, respectively. In the present calculations, we have used the so-called $A = 150$ parameters [17] that appear to give a good understanding of the nuclei in this region [18]. Especially, they have been used in previous studies of ^{140}Nd [3,9].

The configurations in ^{140}Nd are conveniently labeled by the number of high-j particles and holes relative to a $Z = 50$ and

$N = 82$ core,

$$[p_1, n_1 n_2 n_3] \equiv \pi (h_{11/2})^{p_1} \nu (h_{11/2})^{-n_1} \nu (h_{9/2} f_{7/2})^{n_2} (i_{13/2})^{n_3}.$$
$$(1)$$

The number of proton holes in the $g_{7/2}$, $d_{5/2}$ subshells and neutron holes in the $N = 4$ orbitals (mainly the $d_{3/2}/s_{1/2}$ subshells for the yrast states) is then determined from the fixed number of particles, $Z = 60$ and $N = 80$ for ^{140}Nd.

For the low spin states it appears that the $Z = 64$ gap can be considered as closed. This is a reasonable assumption, because the expected deformation of nuclei with $N \leqslant 82$ is rather small, as is also the case for the nuclei with $N > 82$ in which the subshell closure at $Z = 64$ has been established [19]. Therefore it becomes more natural to consider the configurations relative to a ^{146}Gd core. Because the particles (or holes) in the shells between $Z = 50$ and $Z = 64$, $g_{7/2}$ and $d_{5/2}$, are not explicitly listed in the configuration labels as given in Eq. (1), they will remain unchanged. As will become evident below, the levels fed by the isomeric $I = 20$ state are all built from the six holes in the ^{146}Gd core. This is another manifestation of the semimagic properties of the $Z = 64$ core [19], which has been extensively exploited in the description of the terminating bands in the $A = 150$ region [20].

Compared with previous studies [3,9], we have now used an extended formalism [21] with the energy of the observed states normalized to the ground-state mass, which means that not only relative but also absolute observed and calculated energies can be compared. In these calculations, the LSD liquid drop model [22] is used for the ground-state mass with the rigid body moment of inertia calculated from a diffuse surface mass distribution. The aim is to describe the total energy of the high-spin states where pairing should be negligible. Thus, the average pairing energy that is generally included [23] in macroscopic mass formulas is removed. The conclusion of Ref. [21] is that it becomes possible to describe the high-spin states with a similar accuracy as for ground-state masses, i.e., with typical errors somewhat smaller than 1 MeV. Because pairing is neglected in the calculations, a difference is expected at low spin values. This difference should slowly disappear with increasing spin and at high spin values, say $I \gtrsim 30$, we could hope to obtain a more quantitative agreement between calculations and experiment.

In Fig. 7, one notes that up to $I = 20$, the lowest calculated states are formed from four proton holes and two neutron holes in the ^{146}Gd ($Z = 64$, $N = 82$) core, having zero [0,000], one [0,100], and two [0,200] $h_{11/2}$ neutrons in their configurations. Especially, a very favored $I^\pi = 20^+$ state, which was predicted already in Ref. [9], is formed with the angular momenta of all six holes fully aligned. This $I^\pi = 20^+$ state and the states fed by it will be discussed in more detail below. According to the calculations, the yrast states above $I = 20$ up to $I \approx 36$ are then formed from successive excitations of protons across the $Z = 64$ gap to the $h_{11/2}$ subshell. Thus, favored aligned states are formed at $I^\pi = 27^-$, 32^+, and 36^-, i.e., fully aligned states with one [1,200], two [2,200], and three [3,200] $h_{11/2}$ protons. However, in the observed level scheme, there are no states that could be assigned to these favored calculated states. Instead, as concluded previously, the observed yrast states for spin
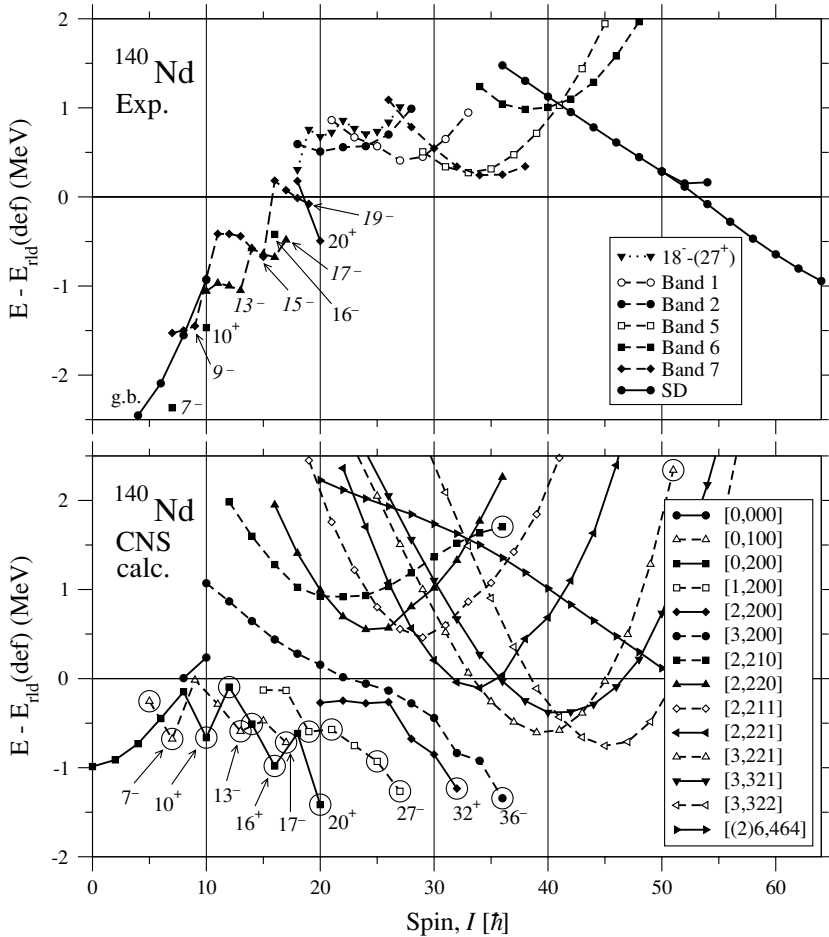
FIG. 7. Experimental and calculated states of ^{140}Nd drawn relative to the same absolute reference so that not only relative but also absolute energies are comparable. The favored spin values of the close to spherical states are indicated. The observed triaxial bands are labeled by numbers according to Ref. [3]. Also shown is one sequence $[18^- - (27^+)]$, which appears to connect between the noncollective states and the triaxial bands, and the superdeformed (SD) bands. The bands calculated in the CNS formalism are identified by the number of high-j particles and holes as detailed in the text.

values $I \approx 20\text{--}40$ can be associated with triaxial bands that are formed if neutrons are excited across the $N = 82$ gap. These configurations result in bands with a typical curvature, i.e., a small second moment of inertia $\mathcal{J}^{(2)}$ when drawn relative to a reference as in Fig. 7. Thus, these bands are in general well understood, although it appears difficult to give any exact configuration assignments. One reason for this is that the parity of these bands is somewhat uncertain as discussed below. Comparing the general features, these bands are calculated too high in energy at low spin values, where pairing correlations are expected to be important. The calculated and observed experimental energies come close together for $I \approx 30$. At even higher spins, the calculated energies are considerably lower than those of the observed bands. This could be caused be deficiencies in the theoretical model, but another possibility is that the observed bands at the highest spins are not yrast, i.e., that there exist lower energy bands for $I \gtrsim 40$ that have not been observed at present.

Finally, also the lower spin states of the superdeformed band are drawn in Fig. 7. Following Ref. [9], it is assumed that the lowest observed state in this band has $I = 36$, in which case it is assigned to the configuration with six $N = 5$ protons and four $N = 6$ neutrons. Considering the slopes in Fig. 7, it appears that the lowest state might have $I = 34$ instead and, as discussed in Ref. [9] another possible configuration is that with one $N = 5$ proton excited into the $N = 6$ orbital, in which

case odd spin values are expected with $I = 37^-$ or 35^- for the lowest observed state.

B. Interpretation of the levels fed by the 20^+ isomer

Because of the neglect of pairing, there is no quantitative agreement between the calculated and observed low-spin states in Fig. 7. Even so, it seems that states at the same spin/parity are favored in experiment and in calculations. Indeed, one can note that the 7^-, 10^+, 13^-, 17^-, and 20^+ states are low in energy. In addition, a relatively low-lying 10^+ state is formed from the $\pi(d_{5/2}g_{7/2})^{-4}$ configuration.

Our interpretation of the low-spin level scheme of ^{140}Nd can be seen as a test of the closed properties of the $Z = 64$ and $N = 82$ core [19]. In the four-proton hole nucleus ^{142}Nd [24] and in the two-neutron hole nucleus ^{144}Gd [25], maximum spin $I^\pi = 10^+$ states have been observed with configurations $\pi(d_{5/2}g_{7/2})^{-4}$ and $\nu(h_{11/2}^{-2})$, respectively. A combination of these two configurations suggests that a maximum spin $I^\pi = 20^+$ state should be formed in the six-hole nucleus ^{140}Nd provided that the "shells are strong enough" so that particle-hole excitations across the gaps will not be strongly favored energetically. It is interesting to compare the six-hole nucleus ^{140}Nd with the six-particle nucleus ^{152}Dy where maximum spin $I^\pi = 27^-$ and 30^+ states based on fully aligned $\pi h(_{11/2})^2 \nu(f_{7/2}h_{9/2})^{3,2}(i_{13/2})^{1,2}$ configurations have

been identified [26]. The energetically favored character of these states is most easily seen when drawn relative to a rigid rotation reference, see, e.g., Ref. [27]. Then even more particles can be added to the core, forming the terminating bands in the $A \approx 155$–160 region [16,20], which have their end points in states with up to 13 particles ($101/2^+$ state in ^{159}Er [28]) or 18 particles+holes (tentative 62^+ state in ^{156}Dy [29]) relative to a ^{146}Gd core.

The level structure of ^{140}Nd at relatively low spin was previously interpreted using shell-model calculations including two-particle-hole excitations with a residual surface δ interaction [6]. The low-lying 7^- and 10^+ states were assigned to the same configurations as suggested from the CNS calculations, i.e., $\nu[h^{-1}_{11/2}d^{-1}_{3/2}]_{7^-}$ and $\nu(h^{-2}_{11/2})_{10^+}$, respectively. In addition, it was found that a rather low-lying 9^- state was formed in an aligned $\nu[h^{-1}_{11/2}(d_{5/2}/g_{7/2})^{-1}]_{9^-}$ configuration and a low-lying aligned 6^+ state in the configuration $\pi[d_{5/2}g_{7/2}]^{-2}_{6^+}$. These states are not straightforward to describe in the CNS formalism, partly because it is difficult to define these pure configurations and for the 9^- state, also because the $\nu(d_{5/2}/g_{7/2})$ subshells appear to be too low in energy.

The main feature of the level scheme above the $I = 9^-$ and $I = 10^+$ states is that the deexcitation follows two parallel cascades of negative parity: one cascade, drawn in the left-hand side of Fig. 1 passes through the favored 13^- and 17^- states at 4700 and 6404 keV, respectively, and the other, drawn in the left-hand side, with a favored 15^- state at 5610 keV and a favored 19^- state at 7483 keV, which is above the 20^+ state and therefore not seen in the delayed coincidences. The separation of the decay in two parallel cascades at medium spins can be related to the different neutron configurations of the contributing four-quasiparticle states: $\nu[h^{-1}_{11/2}(d_{3/2}s_{1/2})^{-1}]$ for the left-hand side cascade of Fig. 1, and $\nu[h^{-1}_{11/2}(d_{5/2}g_{7/2})^{-1}]$ for the right-hand side cascade of Fig. 1.

With this background, we can now conclude that the states of Fig. 1 are naturally understood as built from those configurations which can be formed with four holes in the $Z = 64$ proton core and two holes in the $N = 82$ neutron core, supporting our assumption that this core is not broken when building the states deexcited by the 20^+ isomer.

It is especially the highest spin states within the different configurations that are easy to understand. Thus, as discussed above, with a proton pair broken, $\pi(d_{5/2}g_{7/2})^{-2}$, the maximum spin is 6^+ and with one more pair broken, $\pi(d_{5/2}g_{7/2})^{-4}$, $I_{max} = 10^+$. Similarly, with a neutron pair broken, we can form the configurations $\nu(h^{-2}_{11/2})$, $\nu(h^{-1}_{11/2}d^{-1}_{3/2})$ and $\nu(h^{-1}_{11/2}g^{-1}_{7/2})$ with $I_{max} = 10^+$, 7^-, and 9^-. These states are naturally understood as the observed states at 2365 (6^+), 4155 (10^+), 3619 (10^+), 2221 (7^-), and 3453 (9^-) keV, respectively. These proton and neutron building blocks can then be combined to states with $I_{max} = 13^-$, 15^-, 17^-, 19^-, 20^+, and 16^+ with the configurations spelled out in Table II. It is now interesting to note that different multiplets with highest spins at these values (except for the 16^+ state) can be identified in the observed level scheme. Indeed, it turns out that within an error of typically 100 keV, the energies of the higher spin states can be calculated as simple sums of the energies of the basic building blocks. This is quantified in Table II, where we have

TABLE II. The favored states with $I \leqslant 20$ in ^{140}Nd and their interpretation as simple maximum spin shell-model configurations that can be formed from the six holes in a ^{146}Gd core. The observed energies are given in the third column. In the fourth column, a least-squares fit is made assuming that the energies of the combined states are obtained as sums from the energies of the basic building blocks. In the fifth column, a similar fit is made but excluding the two states involving the $\nu(h^{-2}_{11/2})$ multiplet. No state that is naturally assigned to the predicted 16^+ state is observed, so this state is not included in the fit but the energies that result from the first fit are listed. It might be assigned to the state listed as 16^- in the level scheme. The 4^+ state given in parentheses does not correspond to any observed state but only to the energy required to break a second aligned pair among the four $\pi(d_{5/2}g_{7/2})$ holes, i.e., the energy difference between the 10^+ and 6^+ states.

Configuration	Spin	E_{obs}(keV)	E_{fit}(keV)	E_{fit}(keV)
$\pi(d_{5/2}g_{7/2})^{-2}$	6^+	2365	2329	2347
$+\pi(d_{5/2}g_{7/2})^{-2}$	(4^+)		(1745)	(1789)
$\nu(h^{-1}_{11/2}d^{-1}_{3/2})$	7^-	2221	2307	2280
$\nu(h^{-1}_{11/2}g^{-1}_{7/2})$	9^-	3453	3381	3354
$\nu(h^{-2}_{11/2})$	10^+	3619	3488	
$\pi(d_{5/2}g_{7/2})^{-4}$	10^+	4155	4074	4136
$\pi(d_{5/2}g_{7/2})^{-2}\nu(h^{-1}_{11/2}d^{-1}_{3/2})$	13^-	4700	4636	4627
$\pi(d_{5/2}g_{7/2})^{-2}\nu(h^{-1}_{11/2}g^{-1}_{7/2})$	15^-	5610	5710	5701
$\pi(d_{5/2}g_{7/2})^{-4}\nu(h^{-1}_{11/2}d^{-1}_{3/2})$	17^-	6403	6381	6416
$\pi(d_{5/2}g_{7/2})^{-4}\nu(h^{-1}_{11/2}g^{-1}_{7/2})$	19^-	7483	7455	7490
$\pi(d_{5/2}g_{7/2})^{-4}\nu(h^{-2}_{11/2})$	20^+	7430	7562	
$\pi(d_{5/2}g_{7/2})^{-2}\nu(h^{-2}_{11/2})$	16^+		5817	

made a least-squares fit to these I_{max} states varying the energy of the five building blocks.

The largest discrepancies are for the $\nu(h^{-2}_{11/2})$ 10^+ state and for the 20^+ state, which are the only states where the $\nu(h^{-2}_{11/2})$ configuration enters. Therefore, in the last column, we have made a new fit excluding these two states, then only having four free parameters in the fit, corresponding to the states with spins 6^+, 10^+, 7^-, and 9^- in Table II. The eight I_{max} states within the different configurations are now all obtained with a discrepancy smaller than 100 keV. The fact that additivity works so well indicates that all these states should have about the same deformation. This is also what comes out for those states which can be calculated in the CNS formalism that all have a prolate deformation with $\gamma = -120°$ and $\varepsilon = 0.04$–0.10.

The configuration of the $I = 20^+$ state is illustrated in Fig. 8, where the orbitals calculated in the modified oscillator model (CNS) are drawn at the prolate deformation $\varepsilon = 0.06$. It is then indicated by straight line Fermi surfaces how the four proton holes and the two neutron holes each give a spin contribution of 10^+, resulting in the favored $I = 20^+$ state. Note also that the neutron $d_{3/2}$ subshell is close to the Fermi surface so that also the $\nu(h^{-1}_{11/2}d^{-1}_{3/2})_{7^-}$ state is formed at a favored energy, whereas the $g_{7/2}$ subshell is rather far away from the Fermi surface so that the $\nu(h^{-1}_{11/2}g^{-1}_{7/2})_{9^-}$ state comes out too high in energy in the calculations.
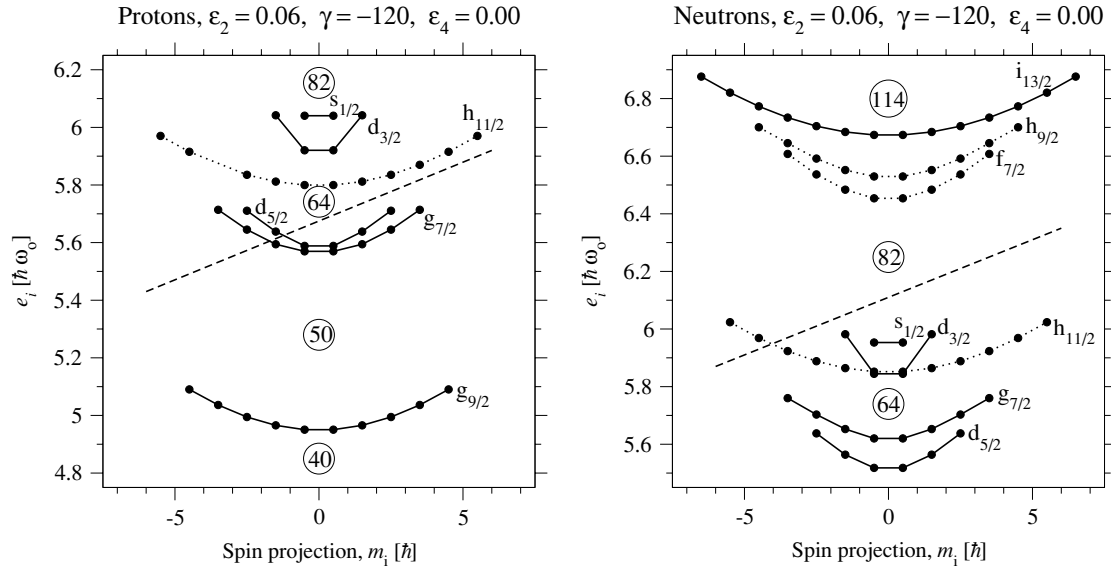
FIG. 8. Tilted Fermi surfaces for protons and neutrons in ^{140}Nd calculated at the relevant prolate deformation $\varepsilon_2 \approx 0.06$. The formation of the proton $(d_{5/2}g_{7/2})^{-4}10^+$ state and the neutron $h_{11/2}^{-2}10^+$ are illustrated by tilted Fermi surfaces.

Even though the spins are not so high, it is very reasonable to neglect pairing for the yrast 20^+ and 17^- states (and also the 19^- state) because they correspond to configurations in a semiclosed $Z = 64$ and $N = 82$ configuration with six orbitals blocked. Indeed, this is also supported by the fact that they are calculated at a too low absolute energy, with a difference that comes close to 1 MeV for the 20^+ state. Therefore, with a substantial pairing energy, the discrepancy would become considerably larger than 1 MeV, which is unexpected from general systematics [21]. It is interesting to compare with the high-spin isomers at $I = 49/2$ and $I = 27$ in the $N = 83$ isotones with $Z =60$–67 where the pairing energy appears to be much less reduced [30]. However, these isomers are built from configurations with particle-hole excitations across the $Z = 64$ and $N = 82$ gaps, which induces substantial deformations ($\varepsilon \approx 0.20$). This is contrary to the 20^+ isomer in ^{140}Nd where, in the absence of pair correlations, no particles are excited across the gaps and all orbitals below the gaps are occupied by one or two particles at a shape that is close to spherical.

It is also interesting to see how the states with $I_{max} - 1, I_{max} - 2, \ldots$ tend to cluster just below the fully aligned states with $I_{max} = 9^-, 13^-, 15^-, 17^-$, and 19^-, which is typical for these kind of shell-model configurations. This is at difference with the situation illustrated for example in Fig. 23 of Ref. [20], where more particles contribute (higher I_{max}): in that case the spacings tend to increase, corresponding to an increased collectivity and the formation of terminating bands.

The 14^- state is somewhat interesting, because it apparently is in common to the two cascades. However, assuming pure $M1$ transitions, we can deduce the branching ratio towards the 13^- states of the two cascades, which is $B(M1; 728)/B(M1; 120) \sim 0.005$. This very small value suggests that the 14^- state belongs to the right-hand side cascade, thus being the $I_{max} - 1$ state of the fully aligned 15^- state. We would then expect also a 14^- state belonging to

the left-hand side cascade, but it has not been observed in the present experiment.

The observed 16^- state in the right-hand cascade at 6154 keV is somewhat difficult to understand in the present interpretation. It connects to states built on the $\nu[h_{11/2}^{-1}(g_{7/2}/d_{5/2})^{-1}]$ neutron configuration. However, the highest spin that can be built if this configuration is combined with a two-proton configuration with spin 6^+ is 15^-, which means that the 16^- state must be based on a four-proton configuration. However, these states with $I = 16^- - 19^-$ appear to start around 600 keV higher in energy. A possibility would then be that the state at 6154 keV has positive parity instead. Indeed, this appears possible from the way it connects to the $15^-, 17^-$, and 18^- states. As the DCO ratio of the 544-keV transition reported in Ref. [3] is 0.46(2), one cannot exclude for this transition an $E1$ character, which will lead to $I = 16^+$. If so, this state could correspond to the $\pi[(d_{5/2}g_{7/2})^{-2}\nu(h_{11/2}^{-2})]_{16^+}$ state that is predicted but not observed. As seen in Table II, the predicted energy comes rather close to 6154 keV. If positive parity is assumed for this state, also the parity of the triaxial bands observed at higher spins in ^{140}Nd should be changed, because they are linked to the 16^+ state by the 1654-keV transition with clear $E2$ character (see Fig. 1 in Ref. [3]). From the theoretical point of view this is not a problem, because no definite interpretation have been given for these bands and configurations of both parities are calculated about equally favored.

C. The unobserved bands terminating at $I^\pi = 27^-, 32^+$, and 36^-

As discussed above, starting from the aligned 20^+ state, favored states are predicted from proton excitations across the semiclosed $Z = 64$ to the high-j $h_{11/2}$ orbitals. If particles and holes are interchanged, these states could be seen

as analogous to the terminating bands and corresponding maximum spin states in ^{152,154,156}Dy [26,29,31], which are formed in configurations with one or a few particle-hole proton excitations relative to the states with all particles outside the ^{146}Gd core fully aligned. In these Dy configurations and also in the predicted ^{140}Nd configurations, no neutrons are excited across the $N = 82$ gap, which means that the deformations stay relatively small. The maximum aligned states with spin 27^-, 32^+, and 36^- in ^{140}Nd are calculated to be yrast by 1–1.5 MeV. Even if we correct for the fact that the aligned low-energy states appears to be calculated somewhat too low in energy relative to the triaxial bands, see Fig. 7, we would still predict that they are of the order 0.5–1.0 MeV below the triaxial bands. Therefore, especially for the 27^- state, it appears strange that it has not been observed. However, considering that the yrast 20^+ state has not been observed in previous experiments, and also the fact that these configurations are expected to have a low collectivity and a nonsmooth E vs. I behavior, it might still not be so strange. Thus, it appears likely that there are indeed lower energy states than those observed in the spin range $I = 20$–36 (or $I = 20$–30) and it would thus be worthwhile to design experiments to try to identify these specific states.

V. SUMMARY

In summary, we have identified a new high-spin isomer at $I^\pi = 20^+$ in ^{140}Nd. Its properties are interpreted using configuration dependent cranked Nilsson-Strutinsky (CNS) calculations as the maximum-spin state that can be formed from the six holes in a ^{146}Gd core. It is thus built from four protons in the $(d_{5/2}, g_{7/2})$ orbitals and two neutrons in the $h_{11/2}$ orbital. This 20^+ state is another manifestation of the subshell closure at $Z = 64$ adding to the systematics

around the ^{146}Gd nucleus, so that maximally aligned hole or particle states have now been observed in the range from ^{140}Nd (6 holes) to ^{159}Er (13 particles outside ^{146}Gd). The lifetime of the isomer is estimated to be larger than the acquisition time gate of $\sim$400 ns.

We showed how the general evolution with spin of the ^{140}Nd level scheme is well understood in the CNS formalism, starting from the shell-model states for $I \leqslant 20$, with a transition to well-developed triaxial bands in the $I = 20$–40 spin range and finally superdeformed bands at the highest spin values. The general features of the shell-model states fed by the 20^+ isomer are well understood as built from the subshells below $Z = 64$ and $N = 82$. We believe that these states would be an ideal laboratory for full shell-model calculations to learn more about the details and also to get a better understanding of the effective interactions appropriate in this region of nuclei. For spin values just above $I = 20$, we predict close-to-spherical yrast states with for example an especially favored 27^- state built as the maximum spin state with one proton excited across the $Z = 64$ gap. These states have not been observed in experiment and it would be interesting to perform some dedicated experiment to learn more about the possible evolution of these close-to-spherical states beyond $I = 20$.

[1] A. Bohr and B. R. Mottelson, *Nuclear Structure* (Benjamin, New York, 1975), Vol. 2.

[2] C. M. Petrache, G. Lo Bianco, D. Ward, A. Galindo-Uribarri, P. Spolaore, D. Bazzacco, T. Kröll, S. Lunardi, R. Menegazzo, C. Rossi Alvarez, A. O. Macchiavelli, M. Cromaz, P. Fallon, G. J. Lane, W. Gast, R. M. Lieder, G. Falconi, A. V. Afanasjev, and I. Ragnarsson, Phys. Rev. C **61**, 011305(R) (1999).

[3] C. M. Petrache, M. Fantuzi, G. Lo Bianco, D. Mengoni, A. Neußer-Neffgen, H. Hübel, A. Al-Khatib, P. Bringel, A. Bürger, N. Nenoff, G. Schönwaßer, A. K. Singh, I. Ragnarsson, G. B. Hagemann, B. Herskind, D. R. Jensen, G. Sletten, P. Fallon, A. Görgen, P. Bednarczyk, D. Curien, G. Gangopadhyay, A. Korichi, A. Lopez-Martens, B. V. T. Rao, T. S. Reddy, and Nirmal Singh, Phys. Rev. C **72**, 064318 (2005).

[4] B. Singh, R. Zywina, and R. B. Firestone, Nucl. Data Sheets **97**, 241 (2002).

[5] G. de Angelis, M. A. Cardona, M. De Poli, S. Lunardi, D. Bazzacco, F. Brandolini, D. Vretenar, G. Bonsignori, M. Savoia, R. Wyss, F. Terrasi, and V. Roca, Phys. Rev. C **49**, 2990 (1994).

[6] E. Gülmez, H. Li, and J. A. Cizewski, Phys. Rev. C **36**, 2371 (1987).

[7] J. Gizon, A. Gizon, M. R. Maier, R. M. Diamond, and F. S. Stephens, Nucl. Phys. **A222**, 557 (1974).

[8] M. Müller-Veggian, H. Beuscher, D. R. Haenni, R. M. Lieder, A. Neskakis, and C. Mayer-Böricke, Nucl. Phys. **A344**, 89 (1980).

[9] A. Neußer, H. Hübel, A. Al-Khatib, P. Bringel, A. Bürger, N. Nenoff, G. Schönwaßer, A. K. Singh, C. M. Petrache, G. Lo Bianco, I. Ragnarsson, G. B. Hagemann, B. Herskind, D. R. Jensen, G. Sletten, P. Fallon, A. Görgen, P. Bednarczyk, D. Curien, G. Gangopadhyay, A. Korichi, A. Lopez-Martens, B. V. T. Rao, T. S. Reddy, and Nirmal Singh, Phys. Rev. C **70**, 064315 (2004).

[10] R. T. Newman *et al.*, Balk. Phys. Lett., Special Issue, 182 (1998).

[11] D. C. Radford, Nucl. Instrum. Methods A **361**, 297 (1995).

[12] L. K. Peker, Nucl. Data Sheets **26**, 473 (1979).

[13] J. C. Merdinger, F. A. Beck, E. Bozek, T. Byrski, C. Gehringer, Y. Schutz, and J. P Vivien, Nucl. Phys. **A346**, 281 (1980).

[14] J. C. Merdinger, Phys. Scr. **24**, 249 (1981).

[15] T. Bengtsson and I. Ragnarsson, Nucl. Phys. **A436**, 14 (1985).

[16] A. V. Afanasjev, D. B. Fossan, G. J. Lane, and I. Ragnarsson, Phys. Rep. **322**, 1 (1999).

[17] T. Bengtsson, Nucl. Phys. **A512**, 124 (1990).

[18] A. V. Afanasjev and I. Ragnarsson, Nucl. Phys. **A608**, 176 (1996).

[19] P. Kleinheinz, R. Broda, P. J. Daly, S. Lunardi, M. Ogawa, and J. Blomqvist, Z. Phys. A **290**, 279 (1979).

[20] I. Ragnarsson, Z. Xing, T. Bengtsson, and M. A. Riley, Phys. Scr. **34**, 651 (1986).

[21] B. G. Carlsson and I. Ragnarsson, submitted to Phys. Lett. B.

[22] K. Pomorski and J. Dudek, Phys. Rev. C **67**, 044316 (2003).

[23] P. Möller, J. R. Nix, W. D. Myers, and W. J. Swiatecki, At. Data Nucl. Data Tables **59**, 185 (1995).

[24] R. Wirowski, J. Yan, A. Dewald, A. Gelberg, W. Lieberz, K. P. Schmittgen, A. von der Werth, and P. von Brentano, Z. Phys. A **329**, 509 (1988).

[25] M. Lach, J. Styczen, R. Julin, M. Piiparinen, H. Beuscher, P. Kleinheinz, and J. Blomqvist, Z. Phys. A **319**, 235 (1984).

[26] M. A. Bentley, A. Alderson, G. C. Ball, H. W. Cranmer-Gordon, P. Fallon, B. Fant, B. Herskind, D. Howe, C. A. Kalfas, A. R. Mokhtar, J. D. Morrison, A. H. Nelson, B. M. Nyakó, K. Schiffer, J. Sharpey-Schafer, J. Simpson, G. Sletten, and P. J. Twin, J. Phys. G **17**, 481 (1991).

[27] I. Ragnarsson, Z. Xing, and T. Bengtsson, Proc. XXIV Int. Winter Meeting on Nuclear Physics, Bormio, Italy, 20-25 Jan. 1986, p. 635.

[28] F. G. Kondev, M. A. Riley, J. Simpson, R. V. F. Janssens, A. V. Afanasjev, I. Ragnarsson, T. B. Brown, D. J. Hartley, M. P. Carpenter, P. Fallon, S. M. Fischer, T. L. Khoo, T. Lauritsen, W. C. Ma, J. F. Sharpey-Schafer, J. C. Lisle, and C. A. Kalfas, J. Phys. G: Nucl. Part. Phys. **25**, 897 (1999).

[29] F. G. Kondev, M. A. Riley, R. V. F. Janssens, J. Simpson, A. V. Afanasjev, I. Ragnarsson, I. Ahmad, D. J. Blumenthal, T. B. Brown, M. P. Carpenter, P. Fallon, S. M. Fischer, G. Hackman, D. J. Hartley, C. A. Kalfas, T. L. Khoo, T. Lauritsen, W. C. Ma, D. Nisius, J. F. Sharpey-Schafer, and P. G. Varmette, Phys. Lett. **B437**, 35 (1998).

[30] A. Odahara, Y. Gono, T. Fukuchi, Y. Wakabayashi, H. Sagawa, W. Satula, and W. Nazarewicz, Phys. Rev. C **72**, 061303(R) (2005).

[31] W. C. Ma, R. V. F. Janssens, T. L. Khoo, I. Ragnarsson, M. A. Riley, M. P. Carpenter, J. R. Terry, J. P. Zhang, I. Ahmad, P. Bhattacharyya, P. J. Daly, S. M. Fischer, J. H. Hamilton, T. Lauritsen, D. T. Nisius, A. V. Ramayya, R. K. Vadapalli, P. G. Varmette, J. W. Watson, C. T. Zhang, and S. J. Zhu, Phys. Rev. C **65**, 034312 (2002).